Galaxy Luminosity functions

- High redshift LF
- Star formation rate at different redshifts

the evolution at $z > 3$ is still (as of 2007) contentious, with some groups claiming that the evolution occurs primarily at the bright end (Shimasaku et al. 2005; B06; Yoshida et al. 2006), others claiming it occurs at the faint end (Iwata et al. 2003, 2007; Sawicki & Thompson 2006a), and still other teams suggesting that the evolution occurs in a luminosity-independent manner (Beckwith et al. 2006). Perhaps the most physically reasonable of these scenarios and the one with the broadest observational support (Dickinson et al. 2004; Shimasaku et al. 2005;B06; Bouwens&Illingworth 2006;Yoshida et al. 2006) is the scenario where evolution happens primarily at the bright end of the LF. In this picture, fainter galaxies are established first and then the brighter galaxies develop later through hierarchical buildup. Observationally, this buildup is seen as an increase in the characteristic luminosity as a function of cosmic time (Dickinson et al. 2004; B06; Yoshida et al. 2006). Less evolution is apparent in the normalization and faint-end slope (B06; Yoshida et al. 2006).

We use the ACS BViz data from the HUDF and all other deep HSTACS fields (including the GOODS fields) to find large samples of star-forming galaxies at z =4 and =5 and to extend our previous z =6 sample. These samples contain 4671, 1416, and 627 B-, V-, and i-dropouts, respectively, and reach to extremely low luminosities [(0:01- 0:04)$L^*_{z=3}$ or M_{UV} =-16 to -17], allowing us to determine the rest-frame UV LF and faint-end slope at z 4-6 to high accuracy.

We find faint-end slopes α= -1.73± 0:05, 1:66 ± 0:09, and 1:74± 0:16 at z =4, 5, and 6, respectively, suggesting that the faint-end slope is very steep and shows little evolution with cosmic time.

We find that M_{UV} brightens considerably in the 0.7 Gyr from z =6 to 4 by 0.7 mag from M^*_{UV} -20:24± 0:19 to -20:98± 0:10).

The observed increase in the characteristic luminosity over this range is almost identical to that expected for the halo mass function, suggesting that the observed evolution is likely due to the hierarchical coalescence and merging of galaxies. The evolution in is not significant.

STY79 DETERMINATIONS OF THE SCHECHTER PARAMETERS FOR THE REST-FRAME UV LFS AT $z \sim 4$, ~ 5, AND ~ 6

Dropout Sample	$\langle z \rangle$	M^*_{UV} [a]	ϕ^* (10^{-3} Mpc^{-3})	α
B [b]	3.8	-21.06 ± 0.10	1.1 ± 0.2	-1.76 ± 0.05
V [b]	5.0	-20.69 ± 0.13	$0.9^{+0.3}_{-0.2}$	-1.69 ± 0.09
i [b]	5.9	-20.29 ± 0.19	$1.2^{+0.6}_{-0.4}$	-1.77 ± 0.16

[a] Values of M^*_{UV} are at 1600 Å for our B- and V-dropout samples and at ~1350 Å for our i-dropout sample. Since $z \sim 6$ galaxies are blue ($\beta \sim -2$; Stanway et al. 2005; B06), we expect the value of M^* at $z \sim 6$ to be very similar ($\lesssim 0.1$ mag) at 1600 Å to the value of M^* at 1350 Å.

[b] Parameters determined using the STY79 technique (§ 3.1) not including evolution across the redshift window of the samples (see Table 7 for the parameters determined including evolution).

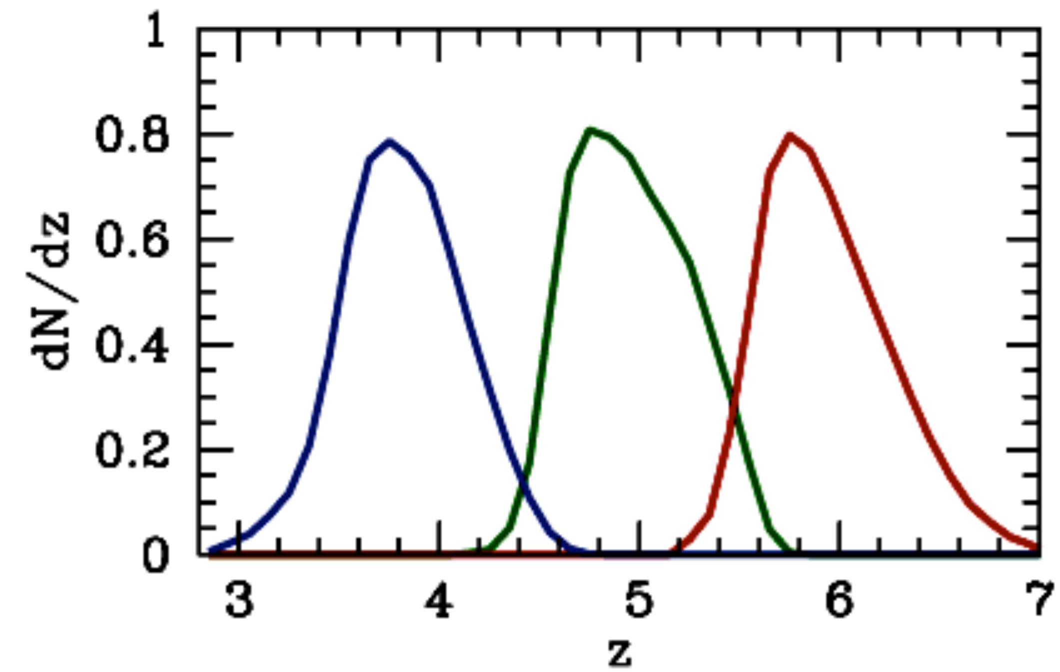

FIG. 2.—Redshift distributions computed for our HUDF B-, V-, and i-dropout samples (*blue, green, and red lines, respectively*) using our best-fit Schechter parameters (Table 4) from the STY79 approach and the selection efficiencies given in Fig. 18. The mean redshift for our HUDF B-, V-, and i-dropout selections is 3.8, 5.0, and 5.9, respectively.

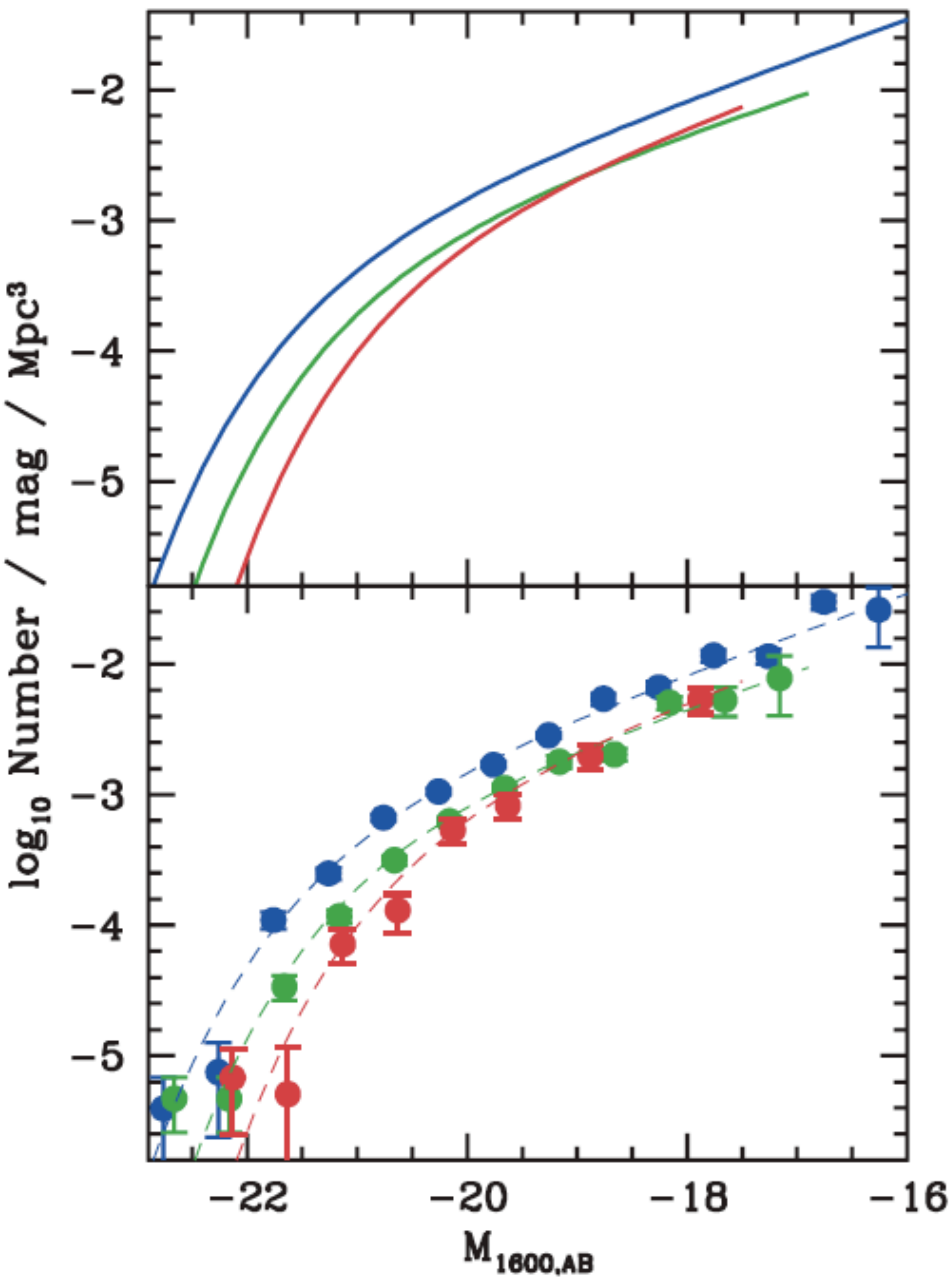

FIG. 4.—*Top*: Rest-frame UV (~1600 Å) LFs at $z \sim 4$ (*blue*), $z \sim 5$ (*green*), and $z \sim 6$ (*red*), shown in terms of their best-fit Schechter functions (*solid lines*), which were derived from fits to the number counts using the STY79 method (§ 3.1). Although nominally our $z \sim 6$ LF requires a *k*-correction to transform it from ~1350 to ~1600 Å, the blue rest-frame UV slopes of $z \sim 6$ galaxies (e.g., Stanway et al. 2005; Yan et al. 2005; B06) mean that the correction is negligible. *Bottom*: Independent determinations of the LFs at $z \sim 4$, ~5, and ~6 using the SWML method (§ 3.2) shown with blue, green, and red filled circles, respectively (1 σ errors). The rest-frame UV LF shows a rapid buildup in the number of luminous galaxies from $z \sim 6$ to ~4. On the other hand, the number of lower luminosity systems ($M_{1600,AB} > -19.5$ mag) shows much less evolution over this interval.

Having derived the rest-frame UV LF at $z \sim 4$, ~ 5, and ~ 6, we can move on to establish the luminosity densities at these epochs. The luminosity densities are of great interest because of their close link to the SFR densities. But, unlike the SFR densities inferred from luminosity density measurements, the luminosity densities are much more directly relatable to the observations themselves, requiring fewer assumptions. As such, they can be more useful when it comes to comparisons between different determinations in the literature, particularly when these determinations are made at the same redshift.

It is common in determinations of the luminosity density to integrate the LF to the observed faint-end limit. Here we consider two faint-end limits: $0.04L^*_{z=3}$ (to match the limits reached by our LF at $z \sim 6$) and $0.3L^*_{z=3}$ (to match the limits reached at $z \sim 7$–10; Bouwens et al. 2004c, 2005; Bouwens & Illingworth 2006).

It is also of interest to convert the luminosity densities into the equivalent *dust-uncorrected* SFR densities using the Madau et al. (1998) conversion factors:

$$L_{\rm UV} = {\rm const}\,\frac{\rm SFR}{M_\odot\ {\rm yr}^{-1}}\ {\rm ergs\ s^{-1}\ Hz^{-1}}, \qquad (3)$$

where const $= 8.0 \times 10^{27}$ at 1500 Å and where a 0.1–125 $M_\odot$ Salpeter initial mass function (IMF) and a constant SFR of $\gtrsim$100 Myr are assumed.

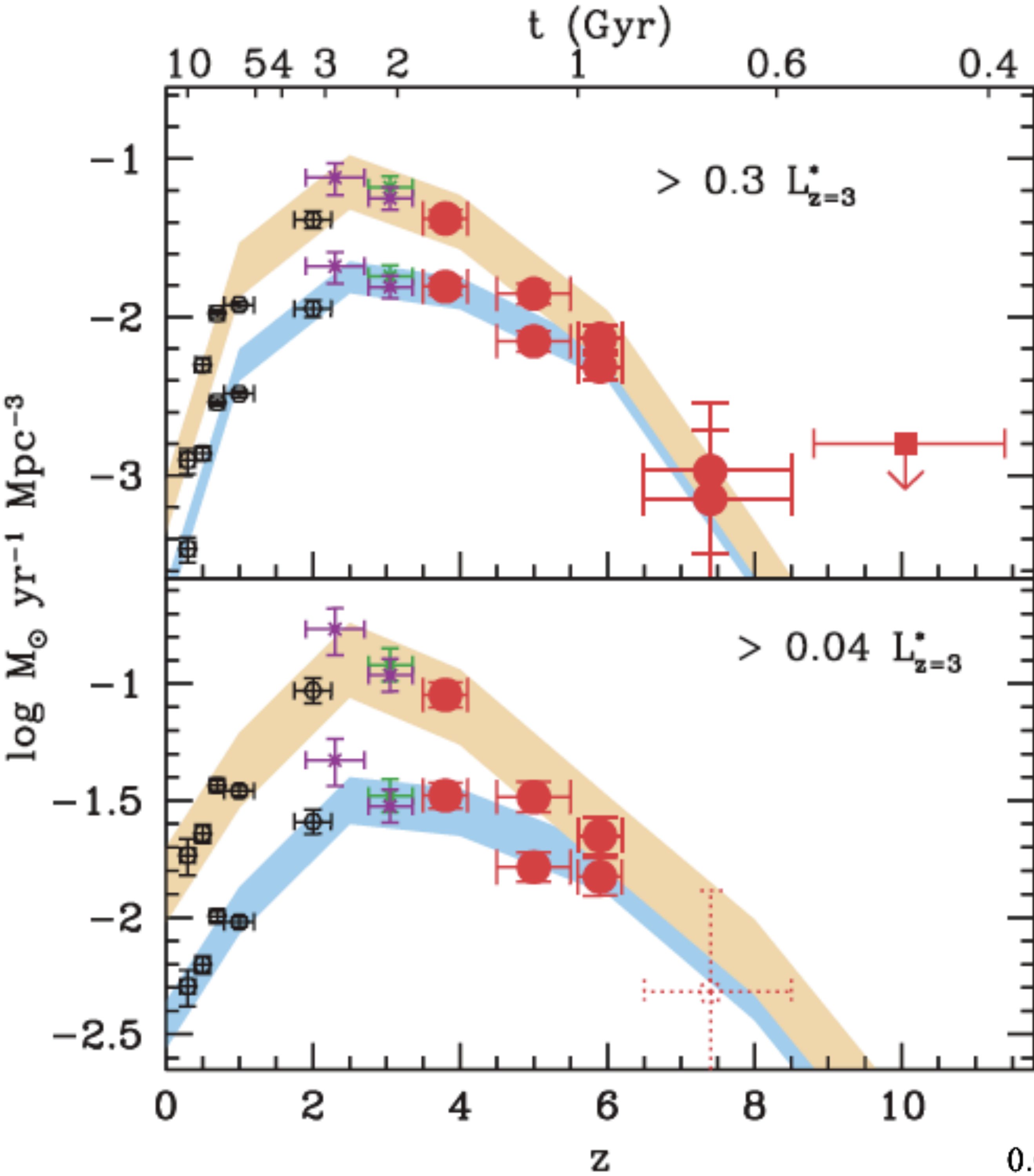

FIG. 7.—SFR density of the universe integrated down to $0.3L^*_{z=3}$ (*top*) and $0.04L^*_{z=3}$ (*bottom*). This SFR density is shown both with and without a correction for dust extinction (*upper and lower set of points, respectively*). This is also indicated with the shaded red and blue regions, where the width of the region shows the approximate uncertainties estimated by Schiminovich et al. (2005). Symbols for the data points are the same as for Fig. 6. At $z \lesssim 3$, the dust corrections we assume are 1.4 mag and are intermediate between the high and low estimates of Schiminovich et al. (2005; 1.8 and 1.0 mag, respectively). At $z \sim 6$, the dust corrections are 0.4 mag as determined from the steep UV continuum slopes (B06). At $z \sim 4$–5, the dust corrections are interpolations between the $z \sim 3$ and ~ 6 values.

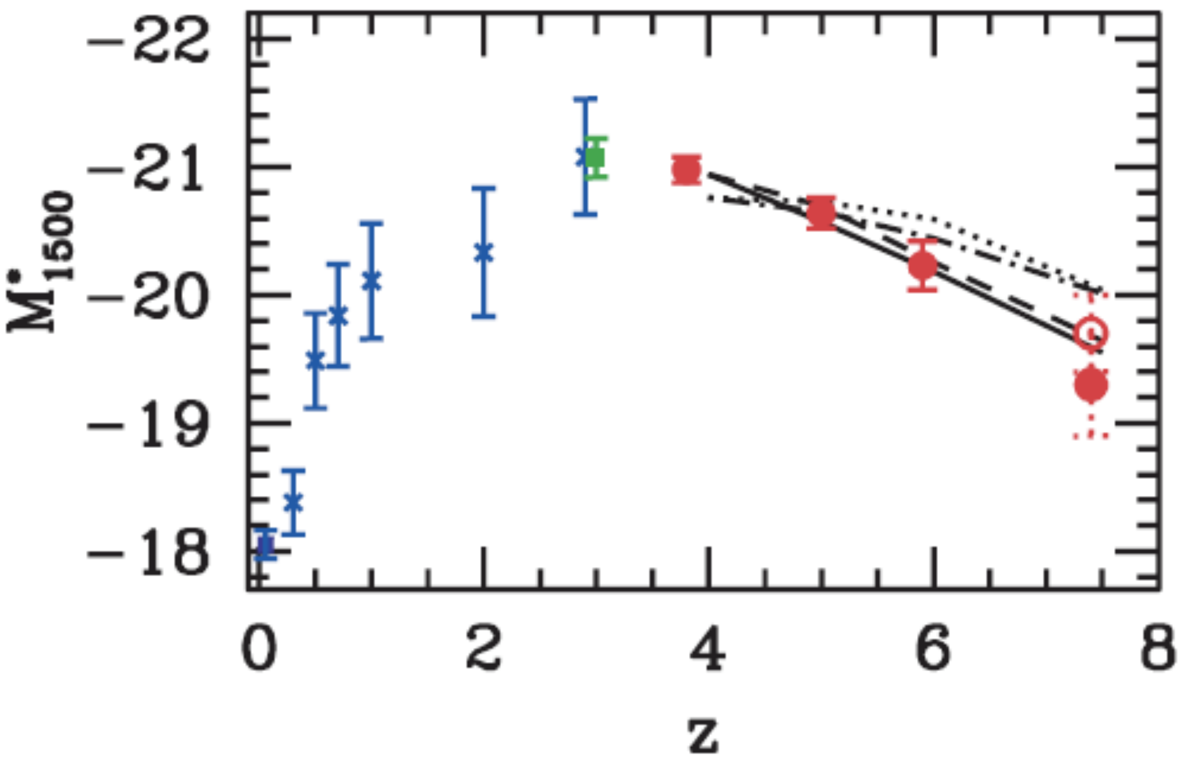

FIG. 13.—Evolution of the characteristic luminosity (M^*) of the UV LF as a function of redshift. Determinations are from the present work at $z \sim 4$–6 (*red circles*), Steidel et al. (1999) at $z \sim 3$ (*green square*), Arnouts et al. (2005) at $0.1 \lesssim z \lesssim 3$ (*blue crosses*), and Wyder et al. (2005) at $z \lesssim 0.1$ (*blue square*). Error bars are 1 σ. See compilation in Table 7. The values of M^* shown at $z \sim 7.4$ (*filled red circle and open red circle, respectively*) are determined (§ 5.2) using the results from the conservative and less conservative z-dropout searches over the two GOODS fields (Bouwens & Illingworth 2006) and assuming that the evolution in the rest-frame UV LF can be accommodated by changes in M^*. The evolution in M^* predicted from the Night et al. (2006) model, the momentum-driven wind model of Oppenheimer & Davé (2006), and the empirically calibrated model of Stark et al. (2007b) are shown as the dotted, dashed, and dot-dashed lines, respectively (see §§ 5.2 and 5.3 for details). The solid line shows the evolution in M^* predicted from the halo mass function (Sheth & Tormen 1999) assuming a constant mass-to-light ratio. To extract a well-defined evolution in M^* with redshift from the models (which resemble power laws in shape), we needed to assume that ϕ^* was fixed, as seen in the observations (Fig. 14). In addition, because the changes we derive for M^* from the models are only differential, the absolute values plotted here are a little arbitrary. The observed characteristic luminosity M^* shows significant evolution at both high and low redshift. At high redshift ($z \gtrsim 4$), the characteristic luminosity brightens very rapidly, reaches a peak at around $z \sim 2$–4, and then fades to $z \sim 0$. The evolution we observe at high redshift in M^* is quite consistent with that found in the halo mass function and in the momentum-driven wind model of Oppenheimer & Davé (2006).

LOWER-LUMINOSITY GALAXIES COULD REIONIZE THE UNIVERSE: VERY STEEP FAINT-END SLOPES TO THE UV LUMINOSITY FUNCTIONS AT $Z \geq 5$-8 FROM THE HUDF09 WFC3/IR OBSERVATIONS[1]

Bouwens et al 2012

The HUDF09 data are the deepest near-IR observations ever, reaching to 29.5 mag. Luminosity functions (LF) from these new HUDF09 data for 132 $z \sim 7$ and $z \sim 8$ galaxies are combined with new LFs for $z \sim 5$-6 galaxies and the earlier $z \sim 4$ LF to reach to very faint limits ($< 0.05\ L^*_{z=3}$). The faint-end slopes α are steep: -1.79 ± 0.12 ($z \sim 5$), -1.73 ± 0.20 ($z \sim 6$), -2.01 ± 0.21 ($z \sim 7$), and -1.91 ± 0.32 ($z \sim 8$). Slopes $\alpha \lesssim -2$ lead to formally divergent UV fluxes, though galaxies are not expected to form below ~ -10 AB mag. These results have important implications for reionization. The weighted mean slope at $z \sim 6$-8 is -1.87 ± 0.13. For such steep slopes, and a faint-end limit of -10 AB mag, galaxies provide a very large UV ionizing photon flux. While current results show that galaxies can reionize the universe by $z \sim 6$, matching the Thomson optical depths is more challenging. Extrapolating the current LF evolution to $z > 8$, taking α to be -1.87 ± 0.13 (the mean value at $z \sim 6$-8), and adopting typical parameters, we derive Thomson optical depths of $0.061^{+0.009}_{-0.006}$. However, this result will change if the faint-end slope α is not constant with redshift. We test this hypothesis and find a weak, though uncertain, trend to steeper slopes at earlier times ($d\alpha/dz \sim -0.05 \pm 0.04$), that would increase the Thomson optical depths to $0.079^{+0.063}_{-0.017}$, consistent with recent WMAP estimates ($\tau = 0.088 \pm 0.015$). It may thus not be necessary to resort to extreme assumptions about the escape fraction or clumping factor. Nevertheless, the uncertainties remain large. Deeper WFC3/IR+ACS

FIG. 1.— The UV luminosity functions at $z \sim 4$, $z \sim 5$, $z \sim 6$, $z \sim 7$ and $z \sim 8$ (§3). The solid circles represent the stepwise maximum-likelihood determinations while the solid lines are the Schechter function determinations (they are *not* fits to the points, though the overall agreement is excellent). The $z \sim 4$ constraints

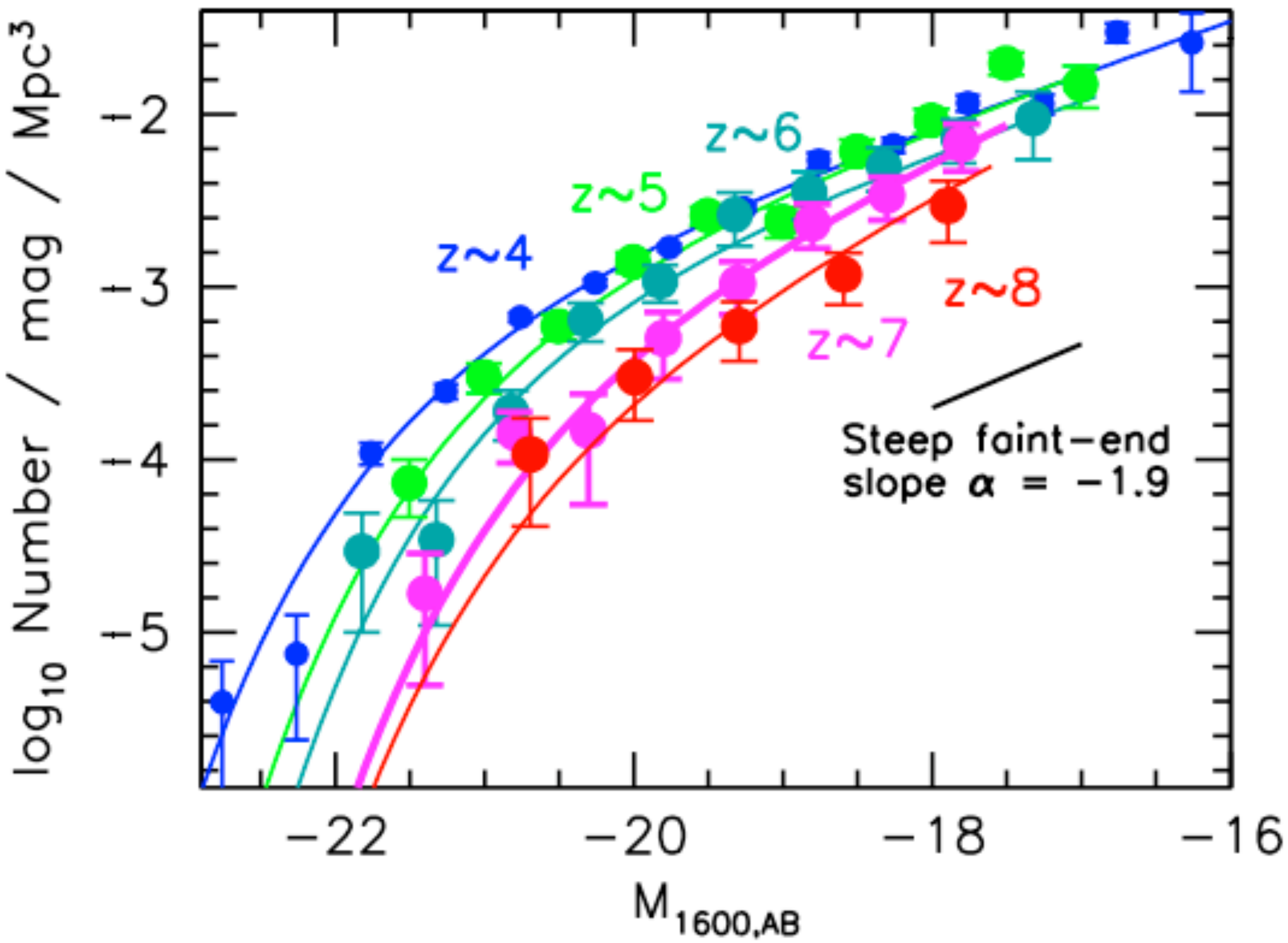

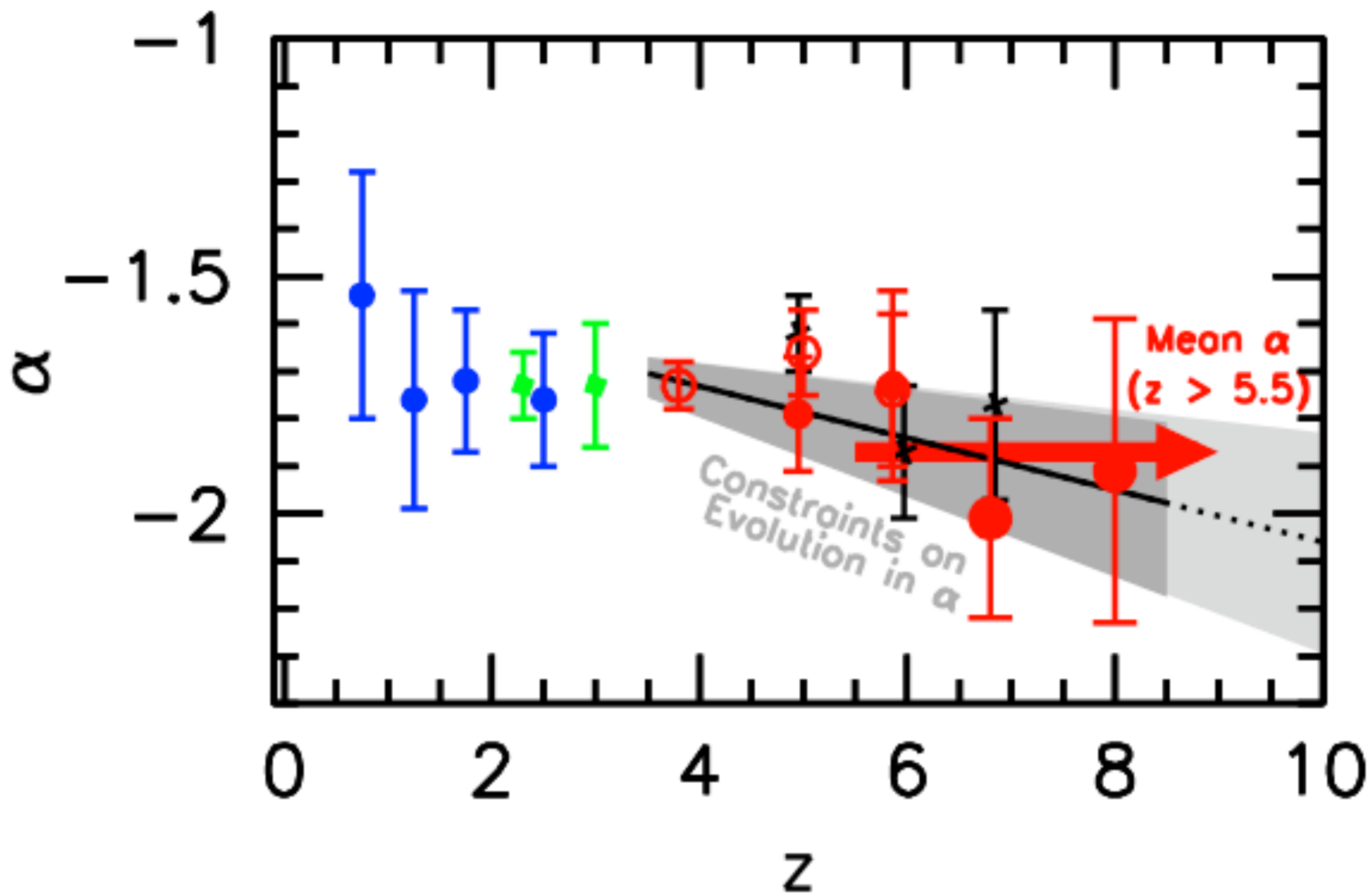

FIG. 2.— Determinations of the faint-end slope α of the UV LF versus redshift (§3; §4). The large solid red points show the new slopes at $z \sim 5$ and $z \sim 6$ from this paper and those at $z \sim 7$ and $z \sim 8$ from Bouwens et al. (2011b). Older determinations are the red open circles at $z \sim 4$, $z \sim 5$, and $z \sim 6$ (Bouwens et al. 2007), black crosses at $z \sim 5$, 6, and 7 (Oesch et al. 2007; Su et al. 2011; Oesch et al. 2010), green squares at $z \sim$ 2-3 (Reddy & Steidel 2009), and blue solid points at $z \sim$ 0.7-2.5 (Oesch et al. 2010c: see also Hathi et al. 2010). Error bars are 1σ. The red horizontal line shows the mean faint-end slope $\alpha = -1.87 \pm 0.13$ we derive at $z \geq 6$. The solid black line is a fit of the $z \sim$ 4-8 faint-end slope determinations to a line, with the 1σ errors (gray area: calculated by marginalizing over the likelihood for all slopes and intercepts). The new WFC3/IR observations provide evidence that LFs at $z \geq$ 5-6 are very steep, with faint-end slopes $\alpha \lesssim -1.8$.

A CENSUS OF STAR-FORMING GALAXIES IN THEZ~9-10 UNIVERSE BASED ON HST+SPITZER OBSERVATIONS OVER 19 CLASH CLUSTERS: THREE CANDIDATE Z~9-10 GALAXIES AND IMPROVED CONSTRAINTS ON THE STAR FORMATION RATE DENSITY AT Z~9.2 Bouwens et al 2013

We utilize a two-color Lyman-Break selection criterion to search for z~9-10 galaxies over the first 19 clusters in the CLASH program. Key to this search are deep observations over our clusters in five near-IR passbands to1.6μm, allowing us good constraints on the position of the Lyman break to z~10. A systematic search yields three z~9-10 candidates in total above a 6σ detection limit.

We find that the normalization of the UV LF at $z \sim 9$ is just $0.22^{+0.30}_{-0.15}\times$ that at $z \sim 8$, $\sim 2^{+3}_{-1}\times$ lower than what we would infer extrapolating $z \sim$ 4-8 LF results. These results therefore suggest a more rapid evolution in the UV LF at $z > 8$ than seen at lower redshifts (although the current evidence here is weak).

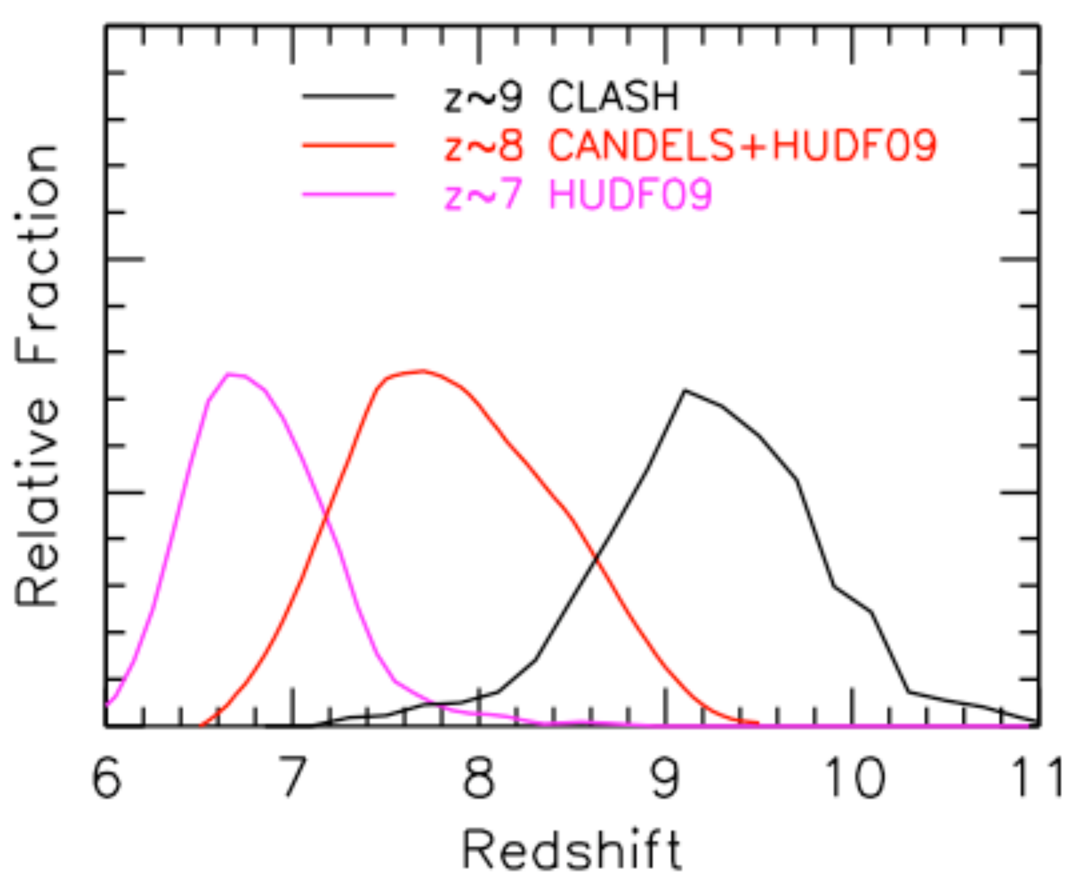

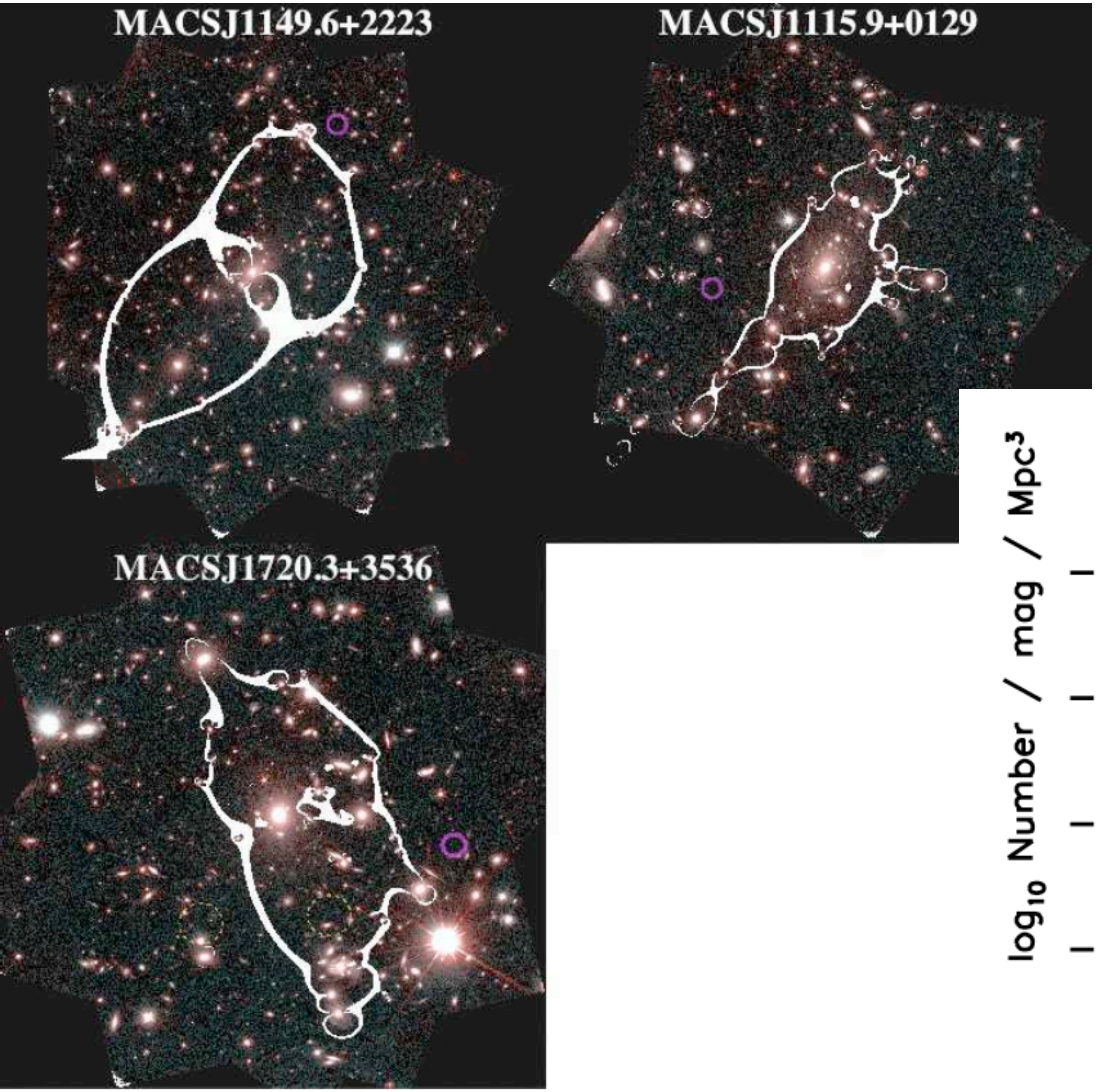

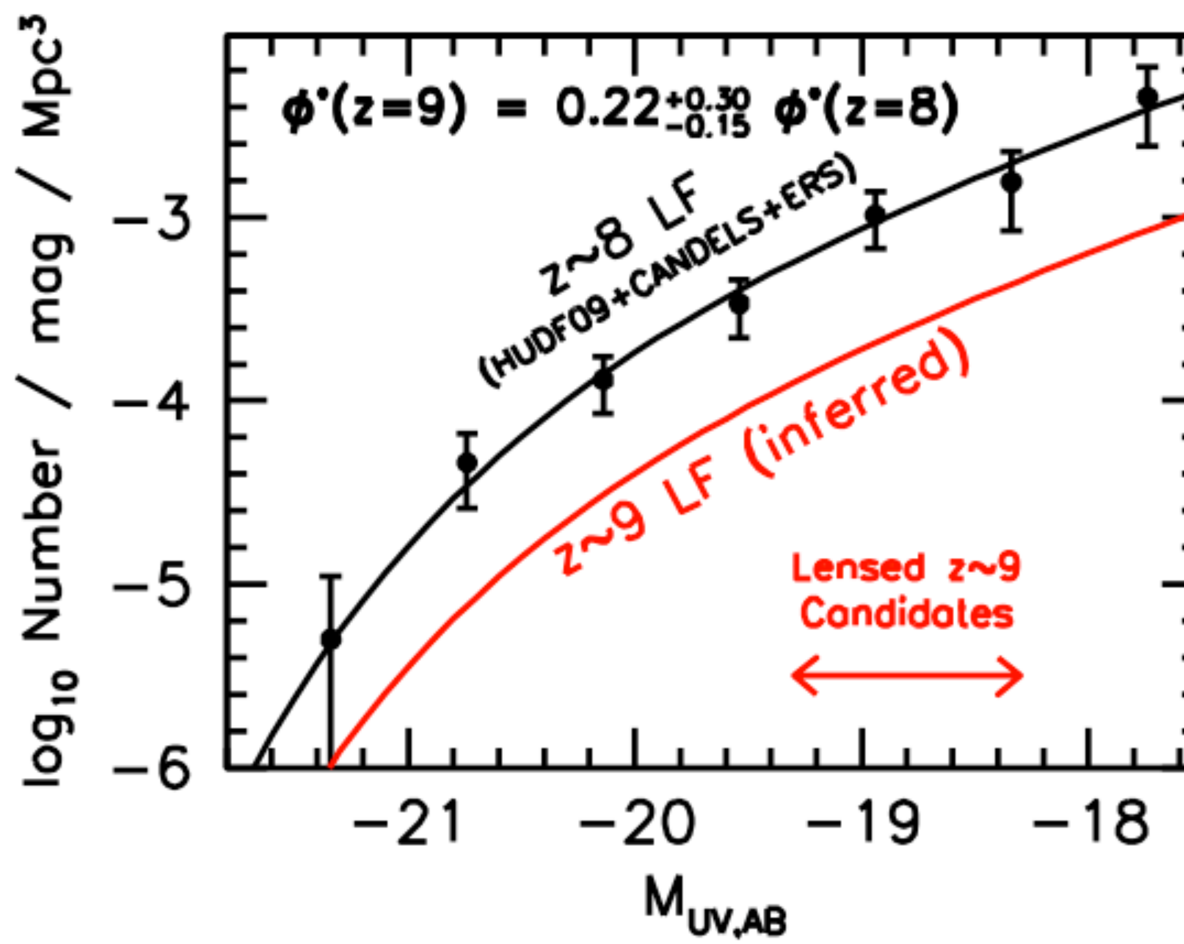

FIG. 4.— Position of the three $z \sim 9$ galaxy candidates we identify over MACSJ1149.6+2223, MACSJ1115.9+0129, and MACSJ1720.3+3536. The color images shown are based on the HST I_{814} + H_{160} observations of these clusters with CLASH and are shown over those regions with deep WFC3/IR observations. Overlaid on these images are the expected ultra high-magnification regions ($\mu > 100$) for a source at $z = 9.2$ based on the gravitational lensing models we have for the three clusters (Z12; A. Zitrin et al. 2012, in prep; M. Carrasco et al. 2012, in prep). Our lensing models for MACSJ1115.9+0129 and MACSJ1720.3+3536 are still preliminary and have not yet been finalized, constructed merely with the assumption that mass traces light, with typically only one lower-redshift system for normalization. The position of our three candidates is indicated by the large magenta circles. The dashed yellow circles indicate the position of possible counterimages as predicted by our preliminary lensing models.

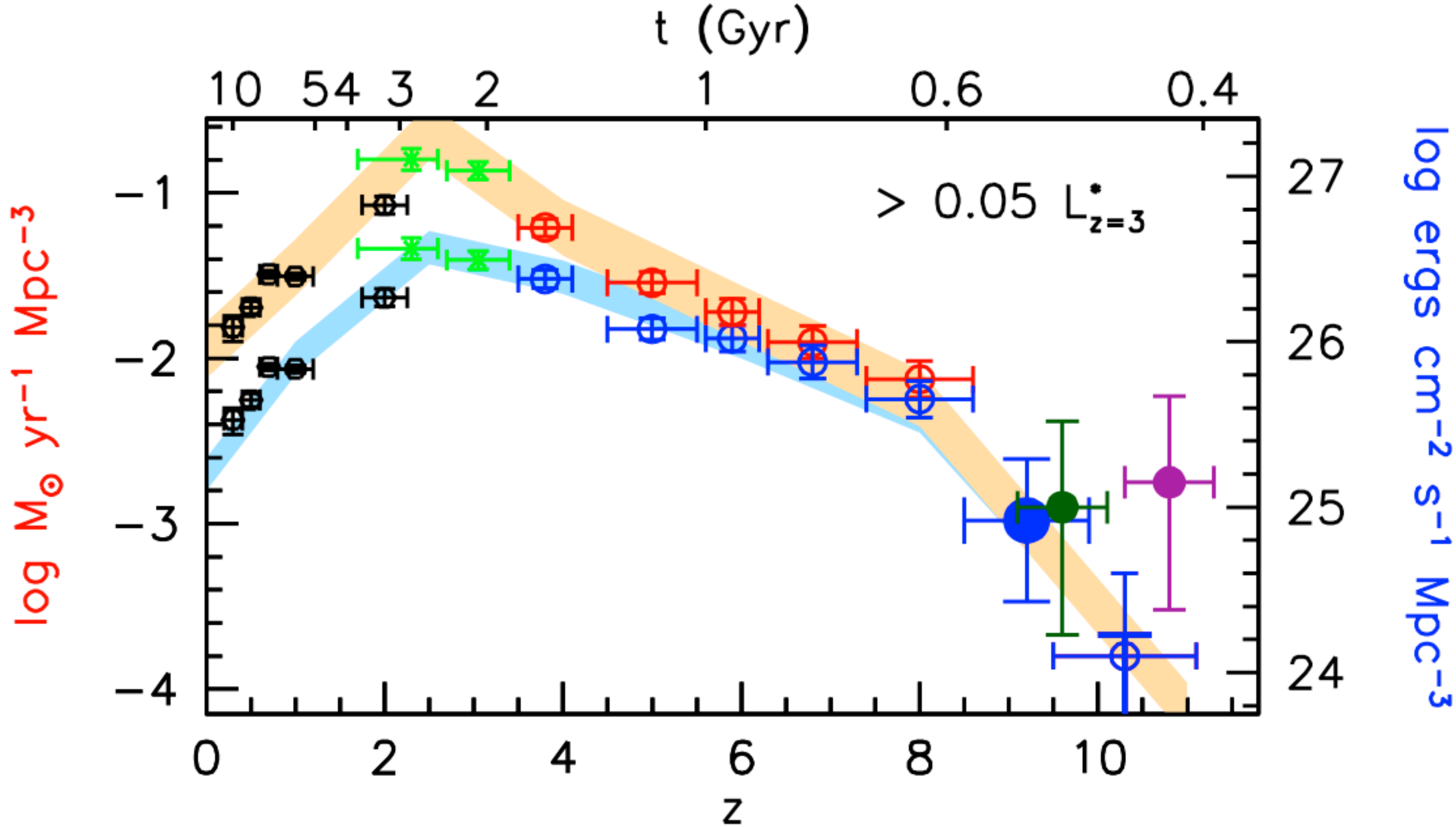

FIG. 10.— The *UV* luminosity density (*right axis*) and star formation rate density (*left axis*) versus redshift. The *UV* luminosity and SFR density shown at $z \sim 9$ (*large blue solid circle*) are from the present work and inferred based on the relative number of $z \sim 8$ and $z \sim 9$ galaxies found within the CLASH cluster program (see §4.5). These luminosity densities and SFR densities are only considered down to a limiting luminosity of −17.7 AB mag – which is the approximate limit of both the HUDF09 probe (Bouwens et al. 2011b) and the present search assuming a maximum typical magnification factor of ∼9 and limiting magnitude of ∼27.0 mag. The *UV* luminosity is converted into a star formation rate using the canonical *UV*-to-SFR conversion factors (Madau et al. 1998; Kennicutt 1998). The upper set of points at every given redshift and orange contour show the dust-corrected SFR densities, while the lower set of points and blue contours show the inferred SFR densities before dust correction. Dust corrections at $z > 3$ are estimated based on the observed *UV*-continuum slope distribution and are taken from Bouwens et al. (2012b). At $z \leq 3$, the dust corrections are from Schiminovich et al. (2005) and Reddy & Steidel (2009). *UV* luminosity density and SFR density determinations from the literature are from Schiminovich et al. (2005) at $z < 2$ (*black hexagons*), Reddy & Steidel (2009) at $z \sim$ 2-3 (*green crosses*, Bouwens et al. (2007) at $z \sim$ 4-6 (*open red and blue circles*), Bouwens et al. (2011b) at $z \sim 7$ (*open red and blue circles*), Oesch et al. (2012b) at $z \sim 8$ (*open red and blue circles*), and Oesch et al. (2012a) at $z \sim 10$ (*open blue circle and upper limit*). Estimates of the SFR density at $z \sim 9.6$ and $z \sim 10.8$ as derived in C12 based on the $z \sim 9.6$ Z12 and $z \sim 10.8$ C12 candidates are also shown (*dark green and magenta solid circles, respectively*). Conversion to a Chabrier (2003) IMF would result in a factor of ∼1.8 (0.25 dex) decrease in the SFR density estimates given here. The present $z \sim 9$ determination is in good agreement with the trend in the SFR density and *UV* luminosity, as defined by the Oesch et al. (2012a) and Z12 estimates.

arXiv:1207.6105

HAM: Basic Approach

1. Choose a stellar mass - halo mass (SMHM) relation from parameter space.

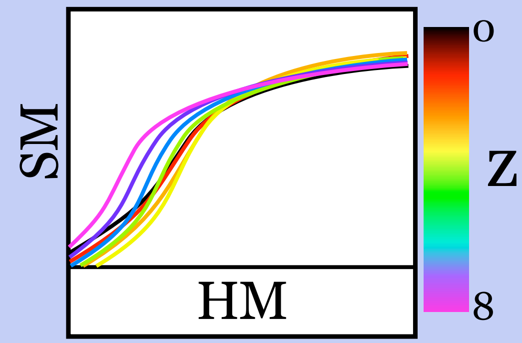

2. Find galaxy growth histories by applying the SMHM relation to dark matter merger trees.

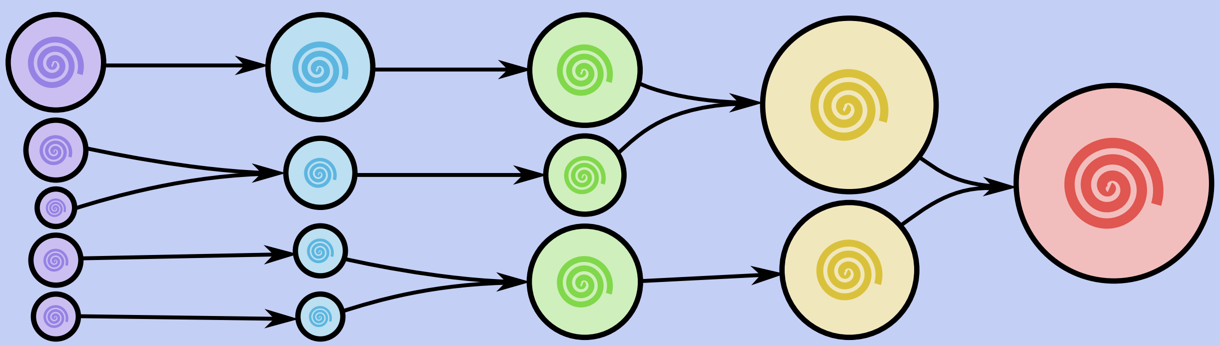

Behroozi, Wechsler, Conroy, 2012

arXiv:1207.6105

Behroozi, Wechsler, Conroy, 2012

Basic Approach

Data Sets:

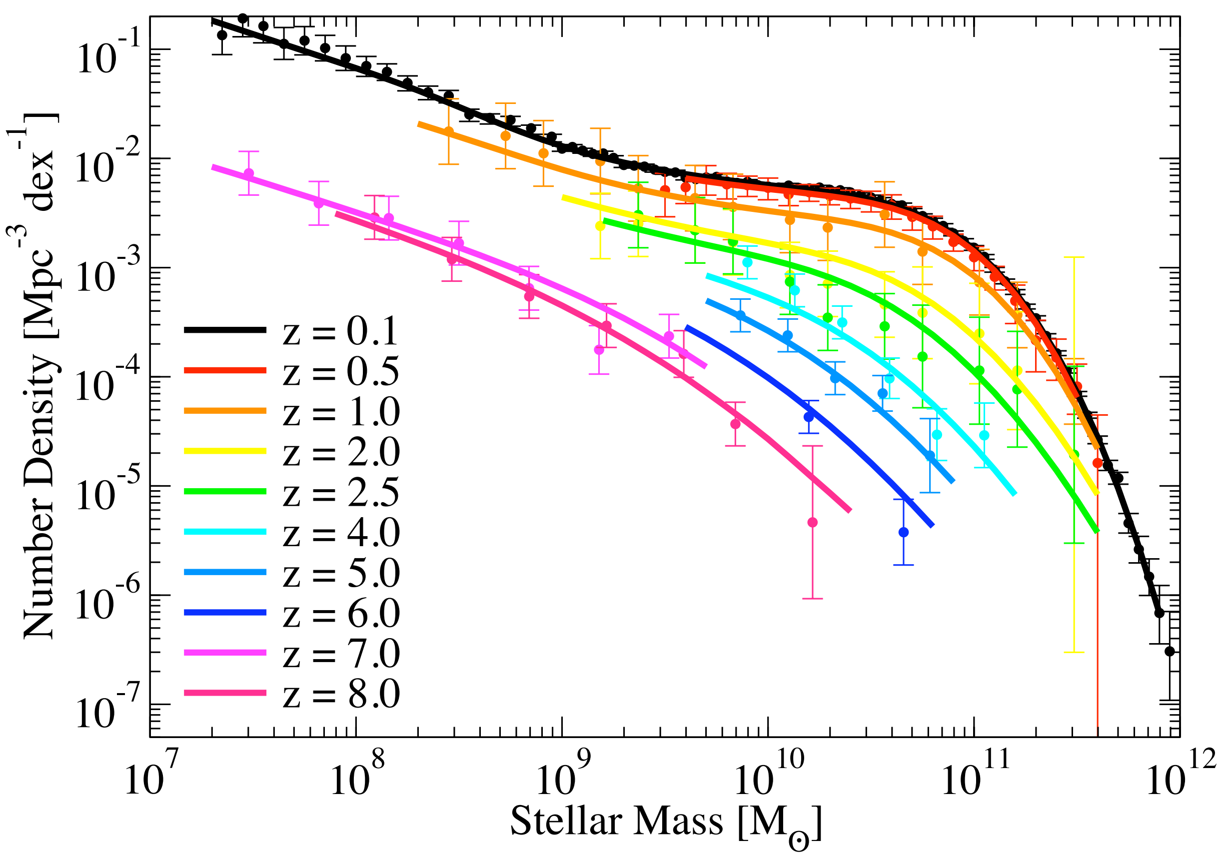

New Stellar Mass Functions from PRIMUS, others up to z=8

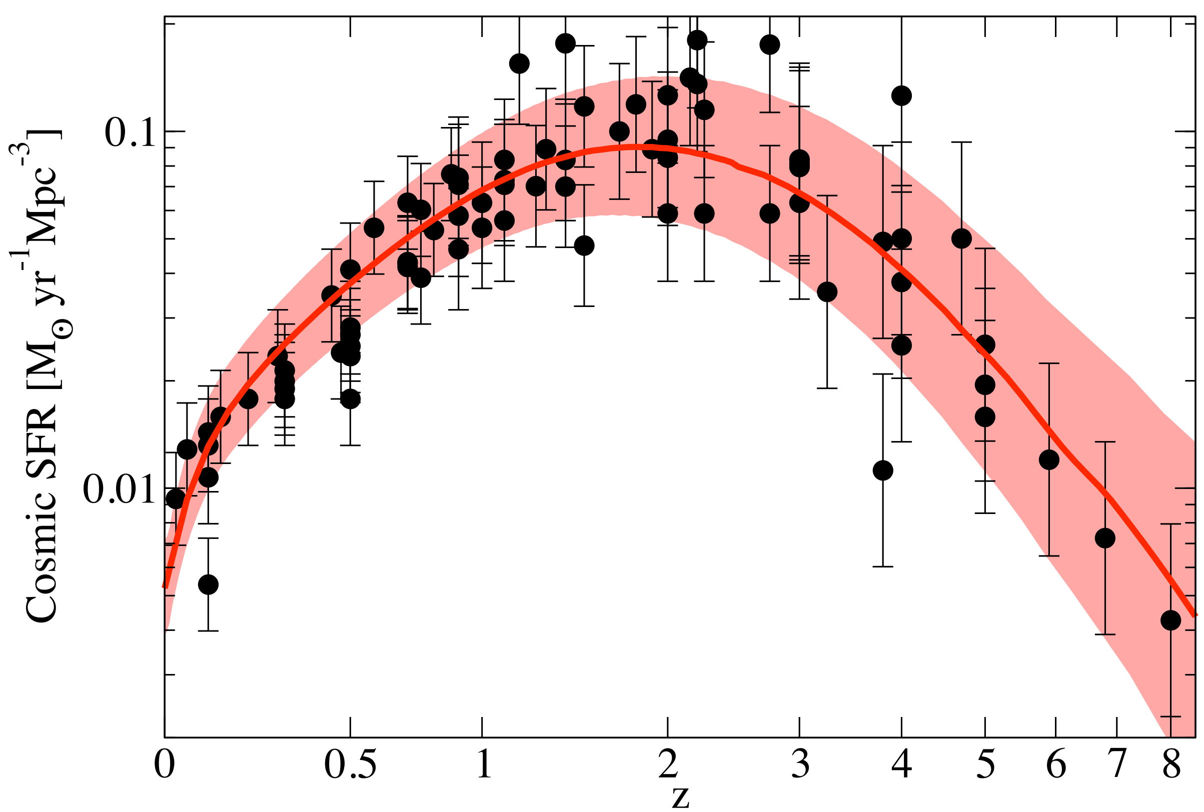

New compilation of cSFRs to z=8

Results

A clear picture of the star formation history of the Universe:

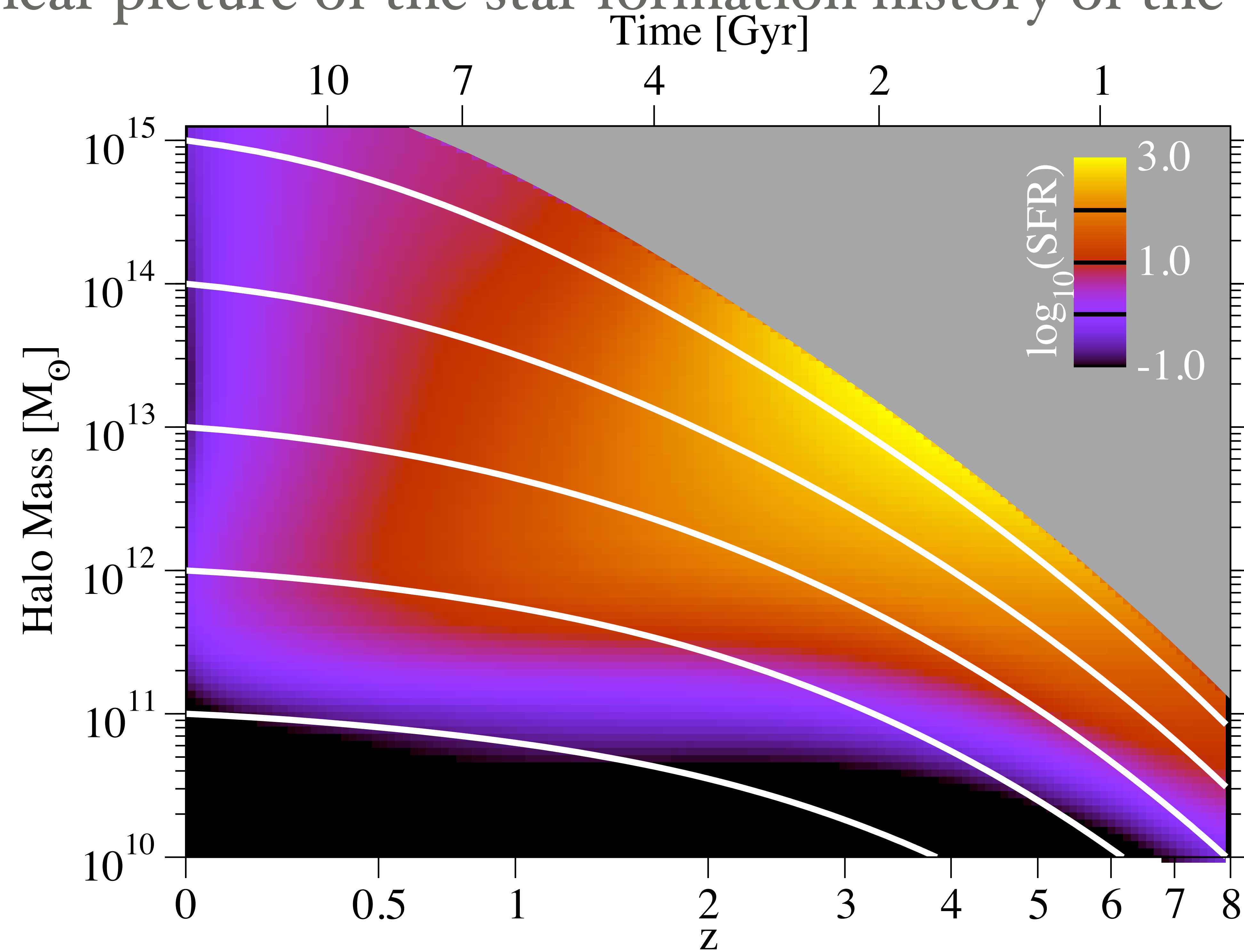

FIG. 4.— The best fitting model (red line) and posterior one-sigma distribution (red shaded region) for the evolution of the specific star formation rate from $z = 0$ to $z = 8$, compared to observational estimates (black points).

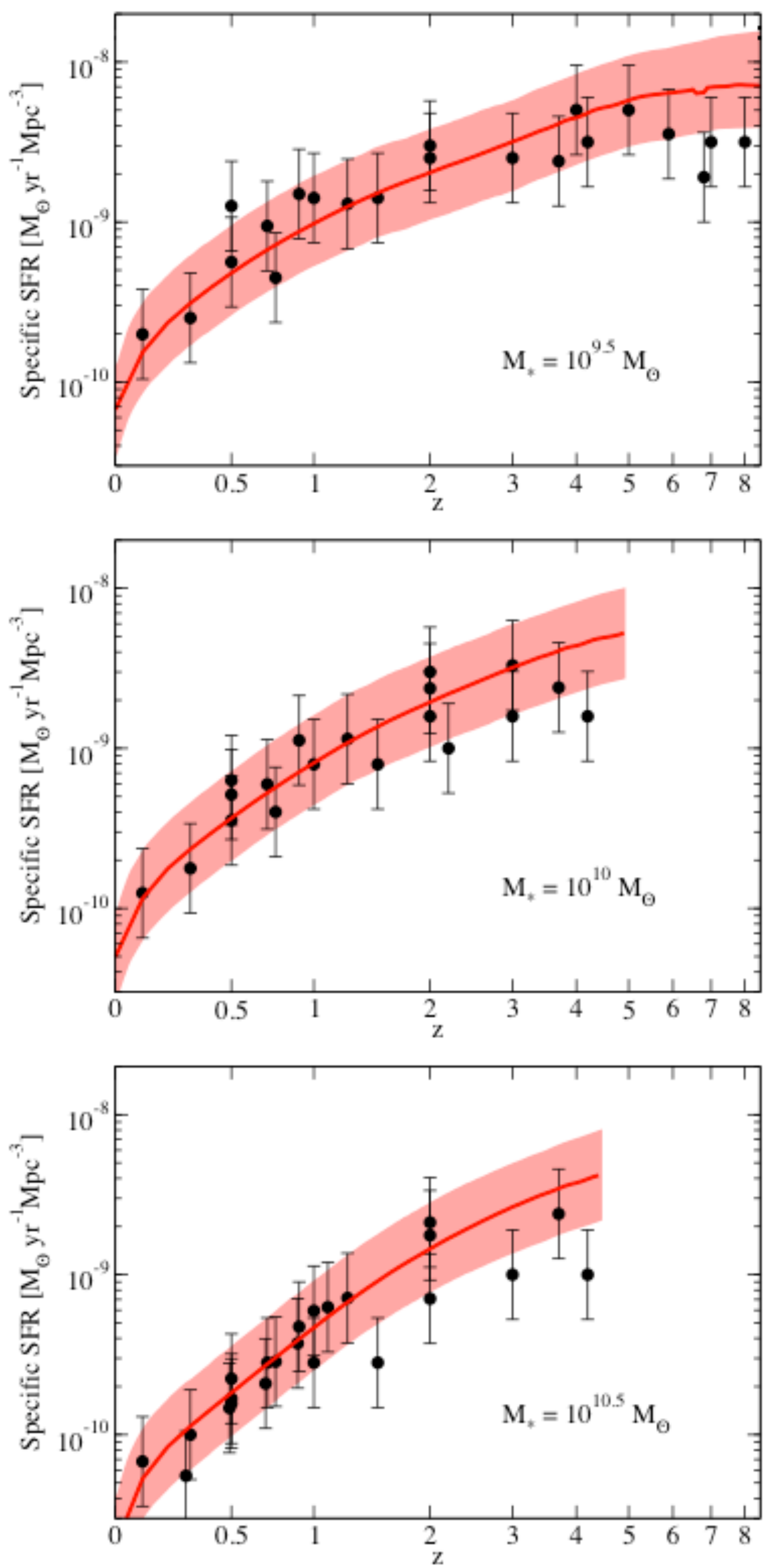

arXiv:1207.6105

Results

Constraints on the M*/Mh ratio, useful for SAMs and hydro:

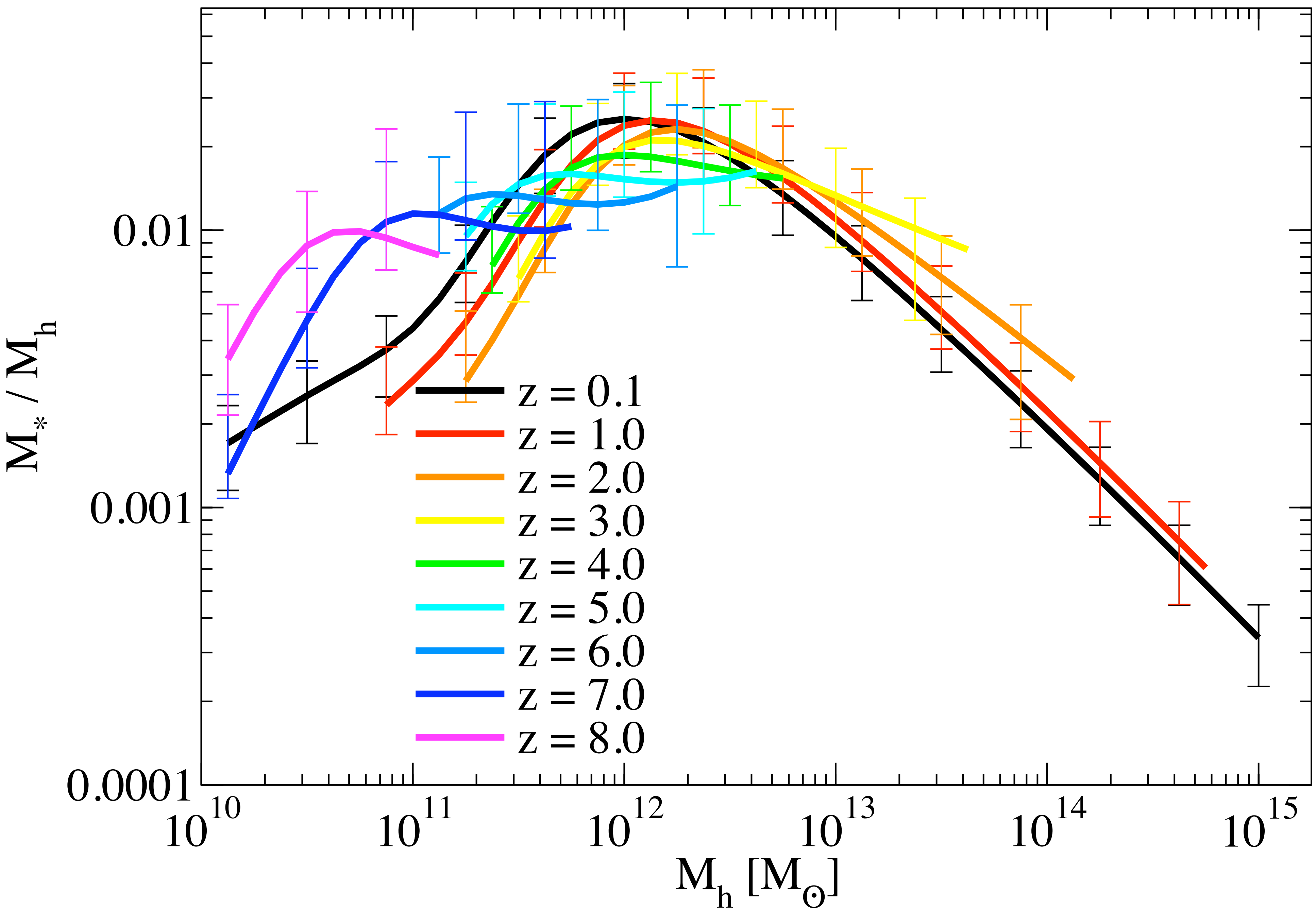

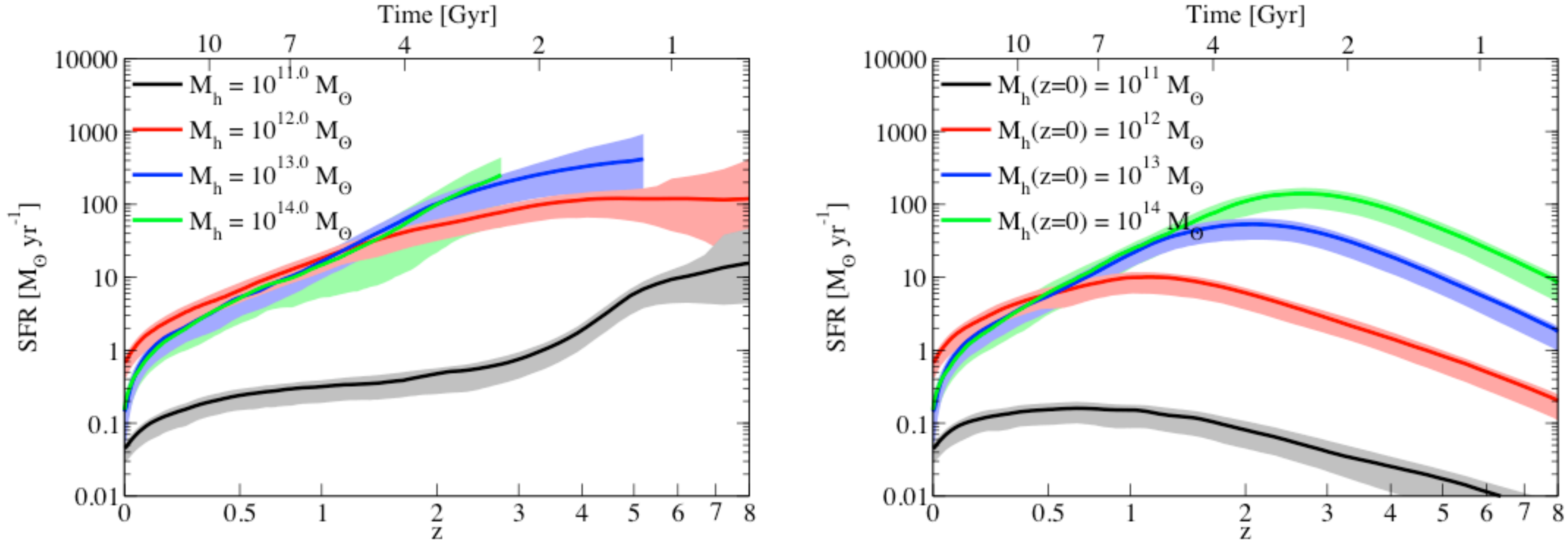

FIG. 6.— **Left** panel: Average star formation rates for the galaxies in halos at a given halo mass and redshift (lines). Shaded regions indicate the one-sigma posterior distribution. **Right** panel: Average star formation histories as a function of halo mass and redshift (lines). Shaded regions indicate the one-sigma posterior distribution. Histories for $10^{15}M_\odot$ halos are not shown as they are very similar to those for $10^{14}M_\odot$ halos.

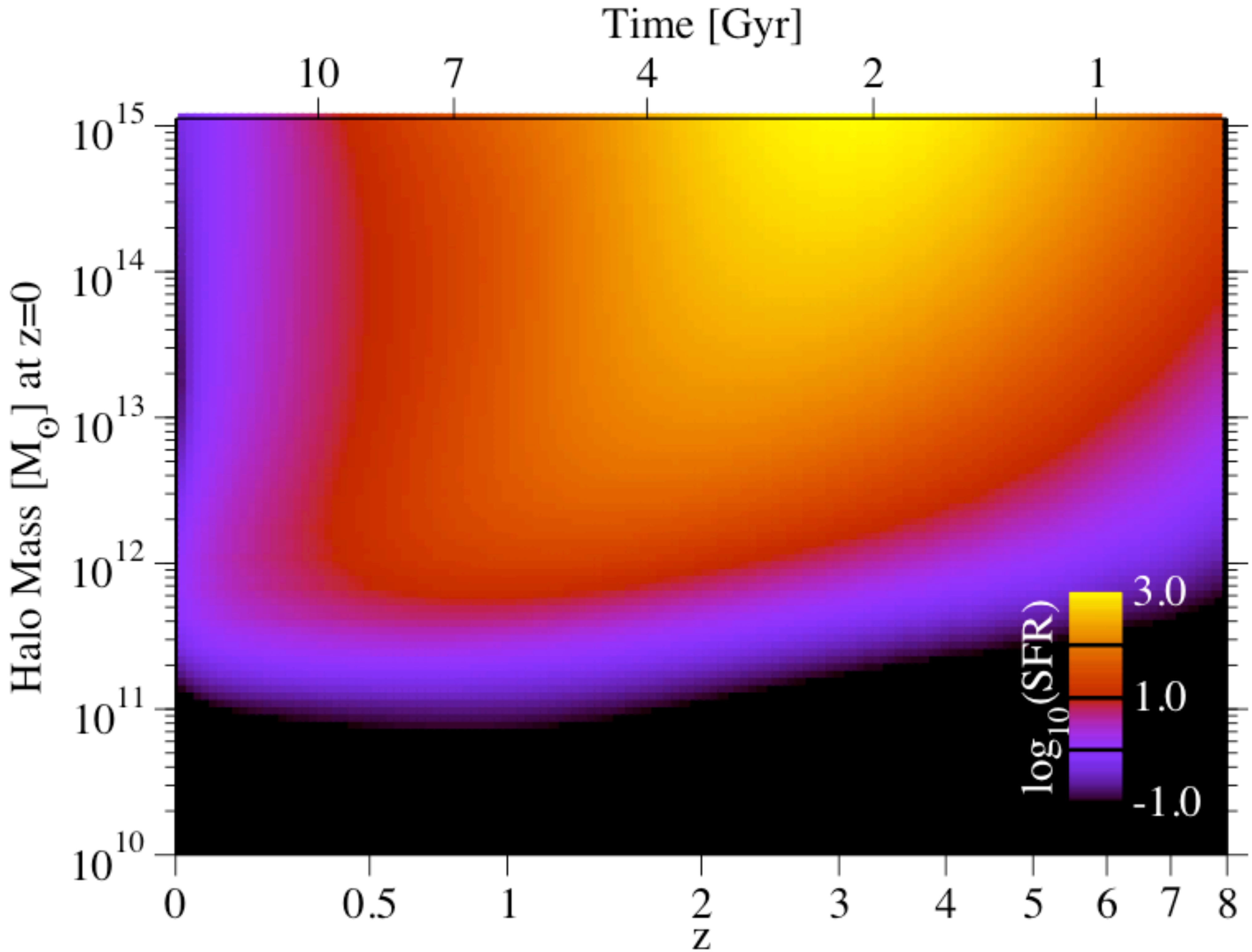

Time [Gyr]
10
7
4
2
1
Halo Mass [M⊙] at z=0
10^{15}
10^{14}
10^{13}
10^{12}
10^{11}
10^{10}
0
0.5
1
2
3
4
5
6
7
8
z
$\log_{10}$(SFR)
3.0
1.0
-1.0

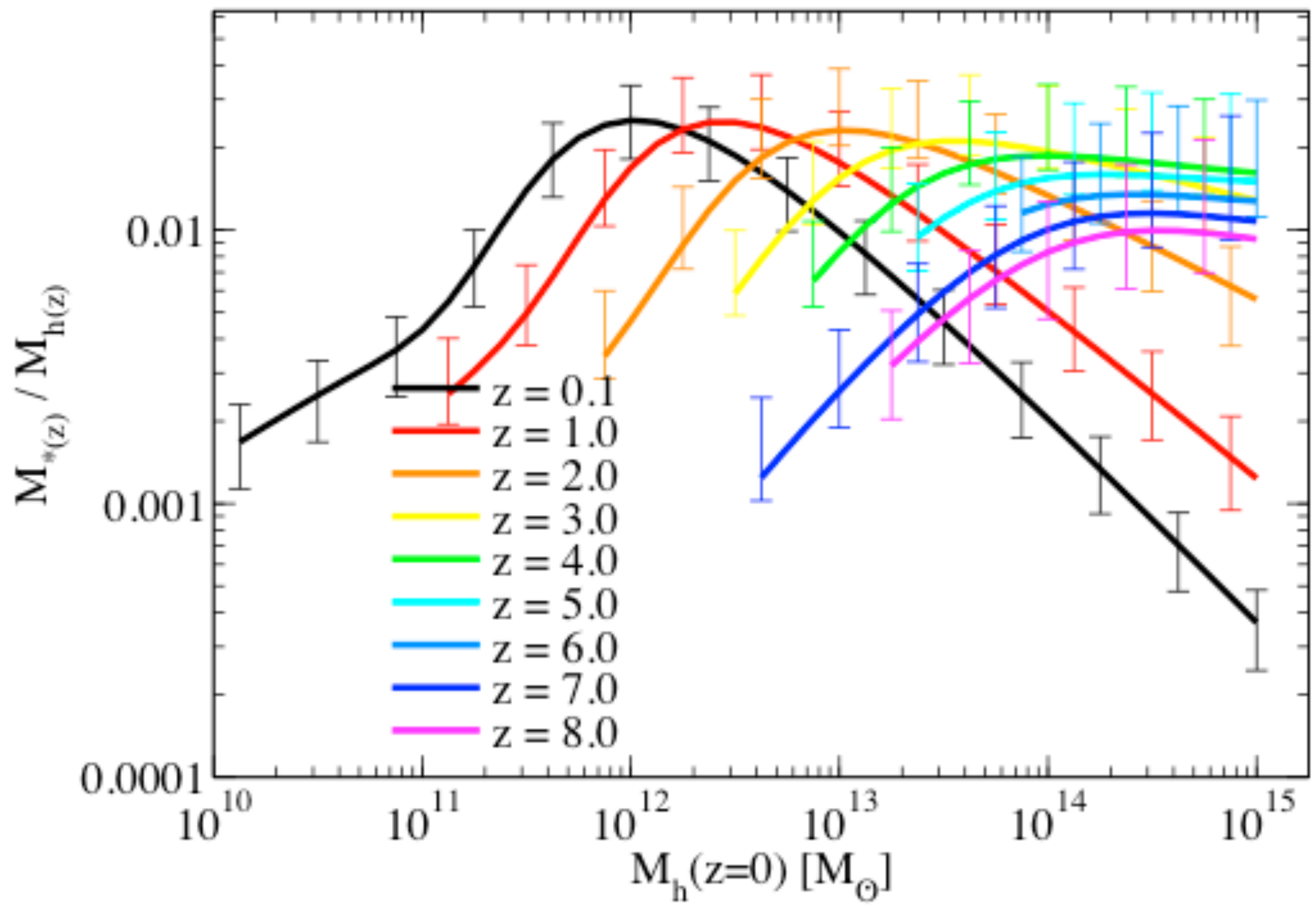

FIG. 8.— Evolution of the derived stellar mass fractions ($M_*(z)/M_h(z)$) as a function of halo mass at the present day. More massive halos used to have a significantly larger fraction of mass in stars, but the peak star formation efficiency has remained relatively constant to the present day.

Stellar-to-Halo mass relation for central galaxies as a function of redshift.

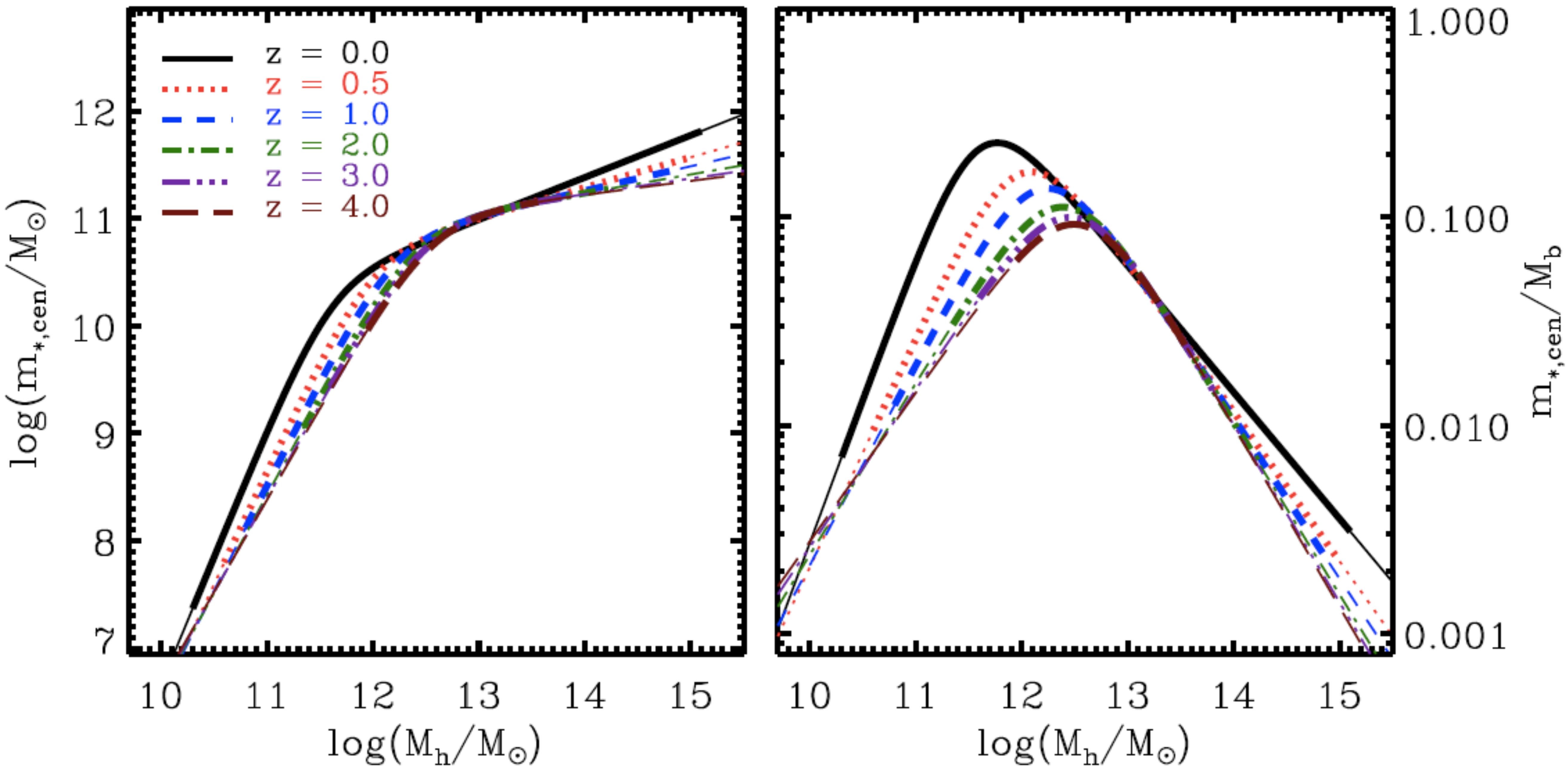

Moster et al 2012